

Full length article

Spectroscopic properties of close-to-perfect-monolayer quasi-free-standing epitaxial graphene on 6H-SiC(0001)

Artur Dobrowolski ^{a,*}, Jakub Jagiełło ^a, Karolina Piętak-Jurczak ^{a,b}, Marek Wzorek ^a, Dariusz Czołak ^a, Tymoteusz Ciuk ^a

^a Lukasiewicz Research Network - Institute of Microelectronics and Photonics, Al. Lotników 32/46, 02-668 Warsaw, Poland

^b Warsaw University of Technology, Faculty of Chemistry, Noakowskiego 3, 00-664 Warsaw, Poland



ARTICLE INFO

Keywords:

Graphene
Epitaxy
CVD
Raman mapping
Spectroscopic ellipsometry
Transmission microscopy
Structural analysis
Layer composition
Topographic imaging

ABSTRACT

In this report, we present transfer-free p-type hydrogen-intercalated quasi-free-standing epitaxial Chemical Vapor Deposition graphene on 15-mm × 15-mm semi-insulating vanadium-compensated on-axis 6H-SiC(0001), characterized in that its room-temperature direct-current Hall-effect-derived hole mobility $\mu_p = 5019 \text{ cm}^2/\text{Vs}$, and its statistical number of layers (N), as indicated by the relative intensity of the SiC-related Raman-active longitudinal optical A_1 mode at 964 cm^{-1} , equals $N = 1.05$. The distribution of the ellipsometric angle Ψ measured at an angle of incidence of 50° and $\lambda = 490 \text{ nm}$ points out to $N = 0.97$. The close-to-unity value of N implies that the material under study is a close-to-perfect quasi-free-standing monolayer, which is further confirmed by High-Resolution Transmission Electron Microscopy. Therefore, its spectroscopic properties, which include the Si-H peak at 2131 cm^{-1} , the histograms of Ψ and Δ , and the Raman G and 2D band positions, widths, and the 2D-to-G band intensity ratios, constitute a valuable reference for this class of materials.

1. Introduction

Transfer-free p-type hydrogen-intercalated [1–5] quasi-free-standing (QFS) graphene grown on semi-insulating (SI), nominally on-axis, hexagonal SiC(0001) in the process of epitaxial Chemical Vapor Deposition (CVD) in argon flow [6], has been appreciated for its reproducible hole density [7,8], thermal stability of transport properties [9,10], scalable growth technology [11], and verified as the optimum graphene platform for monolithic microwave integrated circuits (MMICs) [12–14] and high-temperature Hall effect sensors [9,10,15].

The graphene layer composition is inherently related to the developed surface of the substrate. Although nominally on-axis, the SiC wafer is marked with micrometer-scale terraces separated by few-nanometer-high steps [16,17]. It offers uneven growth conditions favoring additional graphene inclusions at SiC vicinal surfaces [7,8]. A detailed topographic analysis reveals further subtle structural inhomogeneities within the actual (0001) terraces [11,18]. All the above makes each QFS graphene on SiC(0001) sample structurally as unique as a fingerprint.

For these reasons, the number of the graphene layers N that quantifies the specific sample shall not be an integer but a fractional value with a statistical interpretation. To meet this requirement, we had already introduced a truly functional and univalent protocol for layer-resolved imaging and analysis of N based on the shadow the

graphene layers cast on substrate-related Raman-active modes [11, 19]. Specifically, the method assumes that the intensity of the SiC longitudinal optical (LO) A_1 mode at 964 cm^{-1} is attenuated by 2.3 % [20] each time the light passes through a single graphene layer. Upon normalization with respect to a reference graphene-free area, the relative intensity at 964 cm^{-1} measured in a back-scatter geometry is attenuated according to the formula $T(N) = (1 - \pi\alpha)^{2N}$, where $\alpha = 1/137$ is the fine structure constant [20]. We also postulated that the protocol was universal, had supreme differentiation capability, and lifted the limitation of the author's interpretation of the 2D band Full Width at Half Maximum (Δ_{2D}), the 2D-to-G band intensity ratio (I_{2D}/I_G) [11,19] or the G and 2D band positions (ω_G, ω_{2D}).

In this report, we describe the spectroscopic properties of transfer-free p-type hydrogen-intercalated QFS epitaxial CVD graphene on 15-mm × 15-mm SI vanadium-compensated on-axis 6H-SiC(0001), characterized in that its peak value of the LO 964-cm^{-1} mode relative intensity distribution, translates into $N = 1.05$, which is the closest-to-unity value we have ever recorded for this technology. Such a value of N makes us conclude that the material under study is a close-to-perfect QFS monolayer and, therefore, an ideal reference for the entire class of epitaxial QFS graphene.

First, the sample has its room-temperature transport properties verified and functional spectroscopic characteristics assessed. These

* Corresponding author.

E-mail address: artur.dobrowolski@imif.lukasiewicz.gov.pl (A. Dobrowolski).

include high-resolution maps and distributions of the relative intensity of the LO A_1 mode at 964 cm^{-1} , as well as the ellipsometric angles Ψ and Δ . Then, we proceed with traditional non-functional analysis based on A_{2D} , I_{2D}/I_G and ω_G , ω_{2D} . Finally, the discussion is supported with a high-resolution Transmission Electron Microscope (HR-TEM) image of the material cross-section. We argue that the collection constitutes a reference database for possibly close-to-perfect-monolayer QFS epitaxial graphene on 6H-SiC(0001).

2. Experimental details

2.1. Graphene CVD epitaxy and the test structures technology

The hydrogen-intercalated [5] QFS graphene (branded GET) was grown epitaxially on a semi-insulating vanadium-compensated nominally on-axis 500- μm -thick 15-mm \times 15-mm 6H-SiC(0001) sample cut from a 4-in wafer purchased at II-VI Inc. The growth was conducted in a hot-wall Aixtron VP508 reactor at $1600\text{ }^\circ\text{C}$, using Chemical Vapor Deposition in argon flow [6] and thermally decomposed propane as the source of carbon atoms. The flow of argon was adjusted to create optimum conditions for the formation of a boundary layer that simultaneously inhibits the sublimation [21–24] of the top-most silicon atoms from the SiC(0001) surface and enables mass transport of propane. The growth was preceded with *in-situ* etching of the SiC(0001) surface in a purely hydrogen atmosphere at $1600\text{ }^\circ\text{C}$ and chamber pressure of 100 mbar, and followed by *in-situ* hydrogen intercalation at $1000\text{ }^\circ\text{C}$ under 900-mbar argon atmosphere. Shortly after the deposition process, the sample had its statistical room-temperature transport properties assessed over the entire area of the 225 mm^2 by placing four golden probes in the four corners of the sample and using the 0.55-T Ecopia HMS-3000 direct-current Hall effect measurement system.

Next, through a series of optical lithography-based steps involving metal deposition and oxygen plasma etching, the surface of the sample was processed into 63 *van der Pauw* structures, each featuring a cross-shaped [25] 100- μm \times 300- μm QFS graphene mesa against bare 6H-SiC(0001). In this particular experiment, the metallic pads played no electrical role but helped localize the graphene crosses within the sample. An exemplary test structure is depicted in Fig. 1. The optical image is enriched with markings that trace the location of the subsequent Raman mapping, ellipsometric analysis and HR-TEM imaging.

2.2. High-resolution micro-Raman imaging and analysis

The analysis of the relative intensity of the SiC-related Raman-active longitudinal optical (LO) A_1 mode at 964 cm^{-1} , as well as of the graphene-related G and 2D modes, was carried out with Renishaw InVia Raman spectrometer, equipped with the 532-nm (2.33-eV) line of an Nd:YAG laser and a Renishaw CCD detector. The laser beam was projected onto the sample through a $100\times$ objective, and the active modes were fitted with a mixture of Gaussian and Lorentzian line shapes. To enhance the statistical perspective, altogether ten 20- μm \times 15- μm 0.2- μm -step 7676-point Raman maps were collected, each in the same relative location but within a different cross-shaped test structure. The ten structures were chosen evenly out of the 63 fabricated on the sample surface. Each 20- μm \times 15- μm map was oriented in such a way that it comprised a 20- μm \times 10- μm 5151-point QFS graphene-covered area (green marking in Fig. 1) and a 20- μm \times 5- μm 2525-point stripe of exposed 6H-SiC(0001) (beige marking in Fig. 1). The bare 6H-SiC(0001) provided a reference for the intensity of the LO mode at 964 cm^{-1} .

The shadow method was introduced in Ref. [11] and [19]. It draws from the observation that the transmission-mode opacity of a single graphene layer is dependent solely on the fine structure constant α , and defined at $\pi\alpha = 2.3\%$ of the incident visible light [20], while optical transmittance of a stack of N graphene layers follows a negative

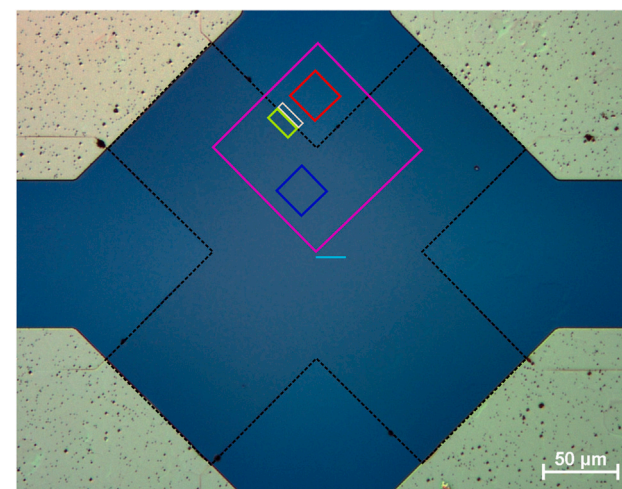


Fig. 1. Nomarski interference contrast optical image of one of the 63 test structures featuring a cross-shaped 100- μm \times 300- μm hydrogen-intercalated QFS epitaxial CVD graphene mesa on semi-insulating vanadium-compensated on-axis 6H-SiC(0001). For clarity, the graphene mesa is marked with a black dashed line. Marked in green is the 20- μm \times 10- μm region intended for high-resolution Raman mapping of graphene, in beige the 20- μm \times 5- μm stripe of referential 6H-SiC(0001), in magenta the 100- μm \times 100- μm region of the ellipsometric analysis, and in blue and red the 25- μm \times 25- μm subareas for the extraction of the Ψ and Δ distributions. The cyan 20- μm line follows the HR-TEM focused-ion-beam cut.

exponential function $T(N) = (1 - \pi\alpha)^N$, regardless of the stacking sequence [26]. In consequence, the intensity of any substrate-related signal, including Raman-active modes, collected in a back-scattered geometry, is attenuated according to the modified formula $T(N) = (1 - \pi\alpha)^{2N}$. As a result, the transmittance is diminished to 95.5% (two times 97.7%) and 91.1% (four times 97.7%) by a single and two graphene layers, respectively. The choice of the reference signal is arbitrary for the reason that the absorption coefficient is almost constant between 500 nm and 750 nm [20]. Yet, for convenience, we choose the SiC LO mode [27] at 964 cm^{-1} .

2.3. Ellipsometric imaging and analysis

Up to date, the ellipsometric characterization has been applied to graphene on 4H-SiC(0001) [28–31], 4H-SiC(0001) [6,29,32], 3C-SiC(111) [33,34], 3C-SiC(111) [29,32–34], and 6H-SiC(0001) [32,35]. Most of these studies targeted the determination of graphene dielectric constants using the Gauss–Newton numerical inversion [36] and the real and imaginary parts of its refractive index using the Kramer–Kronig and Newton–Raphson transformations [30,35,37]. The thickness of the graphene layers on the Si-face of 3C-SiC, 4H-SiC and 6H-SiC was determined using the dielectric function model (MDF) consisting of a Gaussian and Lorentz oscillator [28,32].

Here, the Accurion EP4SE spectral imaging ellipsometer equipped with a Nanochromat NC2 UV–VIS–NIR microscope objective and operating in the nulling regime was used to measure the ellipsometric angles, Ψ and Δ , defined through the ratio ρ of the Fresnel reflection coefficients:

$$\rho = \frac{r_p}{r_s} = \tan\Psi e^{i\Delta}$$

where r_p is the complex reflection coefficient for the electric field vector polarized parallel to the plane of incidence, and r_s is the complex reflection coefficient for the electric field vector polarized perpendicular.

One could expect different conditions for the angle of incidence (AOI) and the wavelength λ in the analysis of Ψ and Δ to meet optimum visual contrast and differentiation capacity between QFS graphene within the cross-shaped mesas and the exposed 6H-SiC(0001) outside

of them. In each case, the AOI was verified between 40° and 68° (with a step of 2°), while the λ between 300 nm and 700 nm (with a step of 5 nm). It was found that Ψ and Δ set very convergent measurement conditions. As a result, the settings were agreed on at $\text{AOI} = 50^\circ$ and $\lambda = 490 \text{ nm}$ for both ellipsometric angles.

A $100\text{-}\mu\text{m} \times 100\text{-}\mu\text{m}$ region of interest was visualized and two $25\text{-}\mu\text{m} \times 25\text{-}\mu\text{m}$ subareas were defined for the extraction of the Ψ and Δ histograms, one of them entirely within the graphene mesa and one within bare 6H-SiC(0001) (as earlier illustrated with magenta, blue and red markings in Fig. 1). The measurements were repeated 10 times and arithmetically averaged to enhance the imaging quality.

To extract the number of the graphene layers N , we adapted a Ψ -devoted work by P. E. Gaskell et al. [38]. In the original publication, the m layers of graphene were considered infinitesimal sheet of optical conductance $m\pi\alpha$, α being the fine structure constant [20], that modifies the Fresnel reflection coefficients r_p and r_s :

$$r_p = \frac{n_1 \cos\theta_i - n_2 \cos\theta_t - m\pi\alpha \cos\theta_i \cos\theta_t}{n_1 \cos\theta_i + n_2 \cos\theta_t + m\pi\alpha \cos\theta_i \cos\theta_t} \quad (1)$$

$$r_s = \frac{n_1 \cos\theta_i - n_2 \cos\theta_t + m\pi\alpha}{n_1 \cos\theta_i + n_2 \cos\theta_t + m\pi\alpha} \quad (2)$$

where n_1 and n_2 represent refractive indices at the phase boundary, and θ_i and $\theta_t = \arcsin(\frac{n_1 \sin\theta_i}{n_2})$, are the angles of incidence and transmission, respectively. Here, the n_1 is associated with the air; therefore, it was set at $n_1 = 1$. The n_2 describes the 6H-SiC substrate and is a purely-real number, as the original work considered only Ψ and anticipated no imaginary parts (extinction coefficients) in the formulae.

Our modification of Eqs. (1) and (2) introduced $2N$ in the place of m since we argue that the detected signal passes each graphene layer twice — once on its way from the light source to the 6H-SiC(0001) surface and once upon its reflection, on its return to the analyzer. Therefore, we postulated the following form of the Fresnel reflection coefficients r_p and r_s :

$$r_p = \frac{n_1 \cos\theta_i - n_2 \cos\theta_t - 2N\pi\alpha \cos\theta_i \cos\theta_t}{n_1 \cos\theta_i + n_2 \cos\theta_t + 2N\pi\alpha \cos\theta_i \cos\theta_t} \quad (3)$$

$$r_s = \frac{n_1 \cos\theta_i - n_2 \cos\theta_t + 2N\pi\alpha}{n_1 \cos\theta_i + n_2 \cos\theta_t + 2N\pi\alpha} \quad (4)$$

2.4. High-resolution transmission electron microscopy

High-resolution cross-sectional imaging of the QFS graphene was performed with the Jeol JEM-2100 Transmission Electron Microscope (TEM) operating at 200 kV. Thin lamellas for the TEM observations were prepared by the Focused Ion Beam (FIB) technique using the FEI Helios 600 NanoLab Dual Beam Microscope equipped with the Omniprobe lift-out system. Since the TEM technique requires the deposition of a thin Pt layer, a process potentially hazardous to graphene, the sample surface was intentionally passivated with an 85-nm-thick [18] amorphous aluminum oxide layer synthesized from trimethylaluminum and deionized water in the process of atomic layer deposition. The sole purpose of the dielectric film was to secure the structural composition of graphene and provide a favorable visual contrast in the HR-TEM image [39].

3. Results and discussion

3.1. Room-temperature transport properties

Fed with direct current I of 1 mA, the sample already proved above-average electrical properties. Its sheet concentration of holes $p_s = 7.69 \times 10^{12} \text{ cm}^{-2}$, in agreement with the theoretically postulated [40–42] and experimentally verified [7,8] $p_s^{6H} \approx 7.5 \times 10^{12} \text{ cm}^{-2}$, its room-temperature direct-current Hall-effect-derived hole mobility $\mu_p = 5019 \text{ cm}^2/\text{Vs}$. Both indicators herald high structural quality of the graphene layer, especially that $\mu_p > 5000 \text{ cm}^2/\text{Vs}$ averaged over the area of 225 mm^2 falls within the 90th percentile of our production stock.

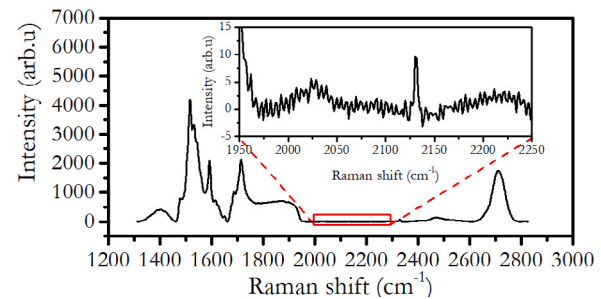


Fig. 2. Arithmetically-averaged Raman spectrum originating from all the $20\text{-}\mu\text{m} \times 10\text{-}\mu\text{m}$ 5151-point Raman maps collected in ten evenly distributed test structures featuring a cross-shaped $100\text{-}\mu\text{m} \times 300\text{-}\mu\text{m}$ hydrogen-intercalated QFS epitaxial CVD graphene mesa on semi-insulating vanadium-compensated on-axis 6H-SiC(0001). The Si-H peak at 2131 cm^{-1} confirms hydrogen presence and a quasi-free-standing character of the graphene.

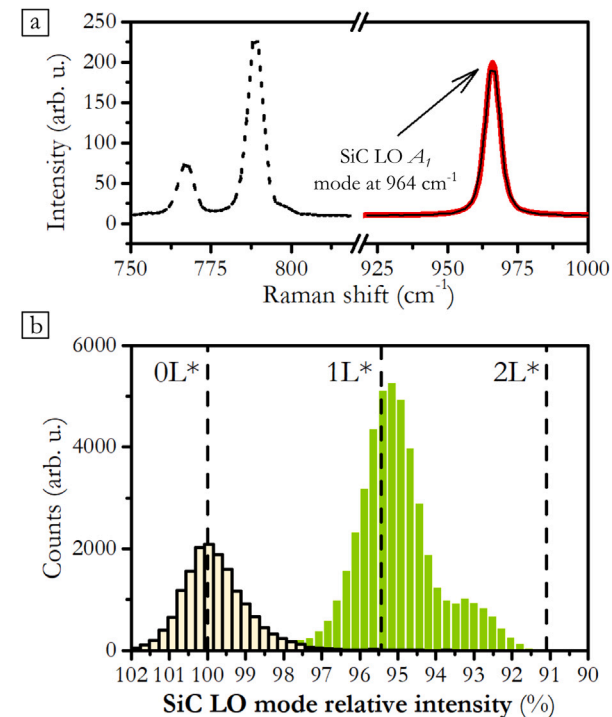


Fig. 3. (a) Exemplary first-order Raman spectrum of 6H-SiC. Marked in red is the longitudinal optical A_1 mode at 964 cm^{-1} (b) Histogram of the 6H-SiC LO A_1 $964\text{-}\text{cm}^{-1}$ mode relative intensity originating from the $20\text{-}\mu\text{m} \times 15\text{-}\mu\text{m}$ 7676-point Raman maps collected in ten evenly distributed test structures featuring a cross-shaped $100\text{-}\mu\text{m} \times 300\text{-}\mu\text{m}$ hydrogen-intercalated QFS epitaxial CVD graphene mesa on semi-insulating vanadium-compensated on-axis 6H-SiC(0001). Marked in green is the QFS graphene-related data, and in beige is the substrate-related data. The vertical dashed lines mark signal attenuation expected for truly single-layer graphene ($1L^*$, $r - I_{\text{SiC}} = 95.5\%$) and truly two-layer graphene ($2L^*$, $r - I_{\text{SiC}} = 91.1\%$).

3.2. Functional and univalent micro-Raman analysis

To prove that the graphene layers are hydrogen-intercalated and indeed quasi-free-standing, a representative spectrum was calculated by arithmetically averaging all single spectra in the ten $20\text{-}\mu\text{m} \times 10\text{-}\mu\text{m}$ 5151-point mesa-related Raman maps. Special attention was paid to the 2131-cm^{-1} Si-H peak, a faint yet unequivocal evidence of successful hydrogenation. The Si-H peak was detected in the averaged mesa-related spectra but not in the reference areas of the exposed 6H-SiC(0001) (Fig. 2).

The functional and univalent analysis of the graphene layer composition was based on the relative intensity of the Raman-active LO A_1

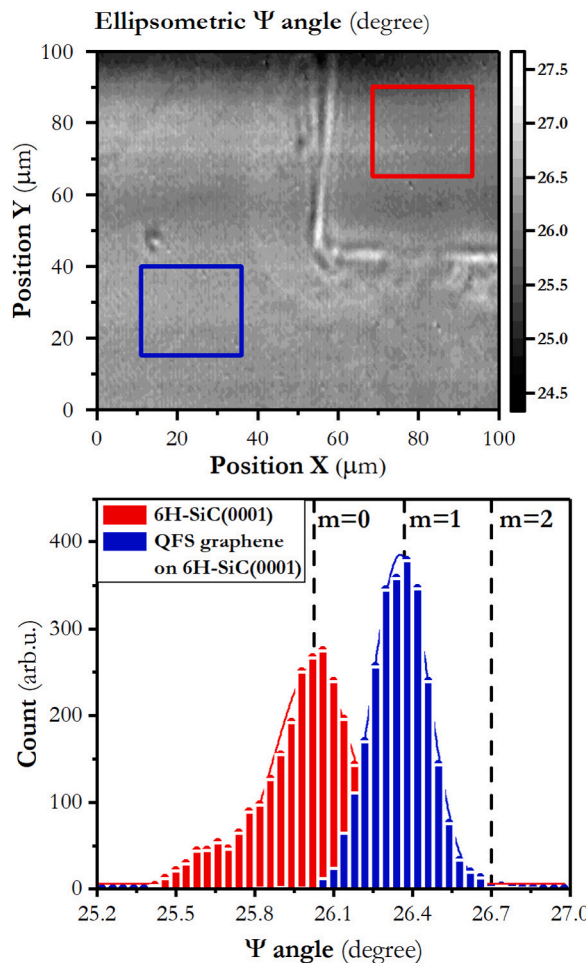


Fig. 4. (a) $100\text{-}\mu\text{m} \times 100\text{-}\mu\text{m}$ topographic map of the ellipsometric angle Ψ , measured at $AOI = 50^\circ$ and $\lambda = 490$ nm, within hydrogen-intercalated QFS epitaxial CVD graphene on semi-insulating vanadium-compensated on-axis $6\text{H-SiC}(0001)$, in accordance with Fig. 1. Marked in blue and red are the $25\text{-}\mu\text{m} \times 25\text{-}\mu\text{m}$ subareas for the extraction of the Ψ distributions within the QFS graphene mesa and the exposed substrate, respectively. (b) Extracted Ψ histograms. The vertical dashed lines indicate Ψ angle expected for a single and two graphene layers based on Eqs. (3) and (4).

mode at 964 cm^{-1} ($r - I_{\text{SiC}}$). Data points originating from the ten $20\text{-}\mu\text{m} \times 15\text{-}\mu\text{m}$ 7676-point Raman maps were collected in a single statistical distribution. It had been already found that regardless of the intensity of the oxygen plasma etching procedure, data points associated with the exposed $\text{SiC}(0001)$ always form a distribution, and by definition they have an easily readable apex and vague tails. For this reason, it is the peak of the referential histogram that we associate with $r - I_{\text{SiC}} = 100\%$.

The graphene-related histogram has its peak value at $r - I_{\text{SiC}} = 95.2\%$, which translates into the statistical number of the graphene layers $N = 1.05$ (marked in green in Fig. 3). The close-to-unity value of N suggests that the material under study is close-to-perfect-monolayer QFS graphene.

3.3. Ellipsometric imaging and analysis

In the domain of Ψ , the data associated with the graphene mesa are located between $\Psi = 25.9^\circ$ and $\Psi = 26.9^\circ$, with the distribution peak at $\Psi = 26.35^\circ$. Data related to the exposed $6\text{H-SiC}(0001)$ span the range between $\Psi = 25.4^\circ$ and $\Psi = 26.6^\circ$, with the peak at $\Psi = 26.02^\circ$. Therefore, the presence of QFS graphene appears to have up-shifted Ψ by 0.33° .

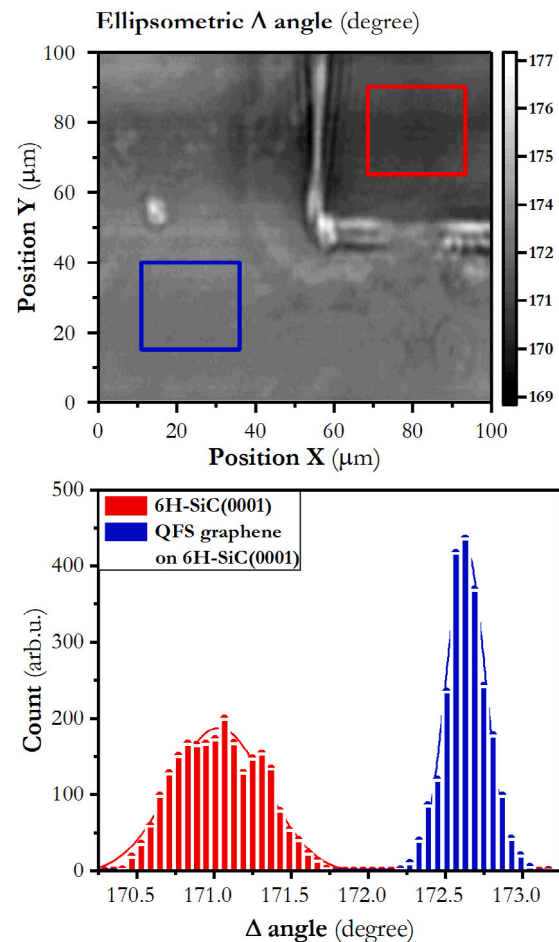


Fig. 5. (a) $100\text{-}\mu\text{m} \times 100\text{-}\mu\text{m}$ topographic map of the ellipsometric angle Δ , measured at $AOI = 50^\circ$ and $\lambda = 490$ nm, within hydrogen-intercalated QFS epitaxial CVD graphene on semi-insulating vanadium-compensated on-axis $6\text{H-SiC}(0001)$, in accordance with Fig. 1. Marked in blue and red are the $25\text{-}\mu\text{m} \times 25\text{-}\mu\text{m}$ subareas for the extraction of the Δ distributions within the QFS graphene mesa and the exposed substrate, respectively. (b) Extracted Δ histograms.

According to the modified model (Eqs. (3) and (4)), $\Psi = 26.02^\circ$ measured at $AOI = 50^\circ$ and $\lambda = 490$ nm outside of the graphene mesa suggests that the real refractive index of the exposed $6\text{H-SiC}(0001)$ is $n_2 = 2.7636$. Based on this, $\Psi = 26.35^\circ$ within the QFS graphene translates into statistically $N = 0.97$ layers, which is comparable with the $N = 1.05$ derived earlier from the Raman analysis (Fig. 4).

In the domain of Δ , the data associated with the QFS graphene mesa are located between $\Delta = 172.2^\circ$ and $\Delta = 173.1^\circ$, with the histogram peak at $\Delta = 172.63^\circ$. Data related to the exposed $6\text{H-SiC}(0001)$ span the range between $\Delta = 170.4^\circ$ and $\Delta = 171.7^\circ$, with a peak at $\Delta = 171.03^\circ$. Therefore, the up-shift of Ψ by 0.33° is associated with the up-shift of Δ by 1.60° (Fig. 5). Although we do not translate the Δ distribution into the number of the layers N , it is apparent that the presence of graphene affects Δ a greater extent than Ψ .

3.4. Non-functional micro-Raman analysis

The traditional, non-functional analysis of the graphene layer composition was based on distributions of the second-order Raman 2D peak [43,44] width A_{2D} , the 2D-to-G band intensity ratio I_{2D}/I_G , and data clouds of the G and 2D band positions ω_G , ω_{2D} .

The 2D peak width spans a relatively extensive range between 45 cm^{-1} and 65 cm^{-1} , with an expected value of 53.6 cm^{-1} . Interestingly, all data points previously associated with the LO A_1 mode

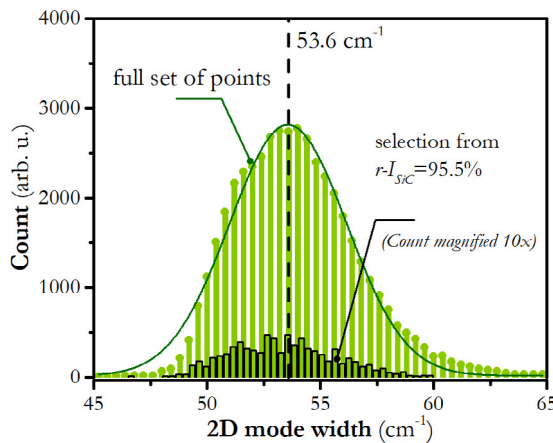


Fig. 6. Histogram of 2D band width originating from the 20- μm \times 10- μm 5151-point Raman maps collected in ten evenly distributed test structures featuring a cross-shaped 100- μm \times 300- μm hydrogen-intercalated QFS epitaxial CVD graphene mesa on semi-insulating vanadium-compensated on-axis 6H-SiC(0001). Marked out with a black rim is data associated with $r - I_{SiC} = 95.5\%$ (1L*).

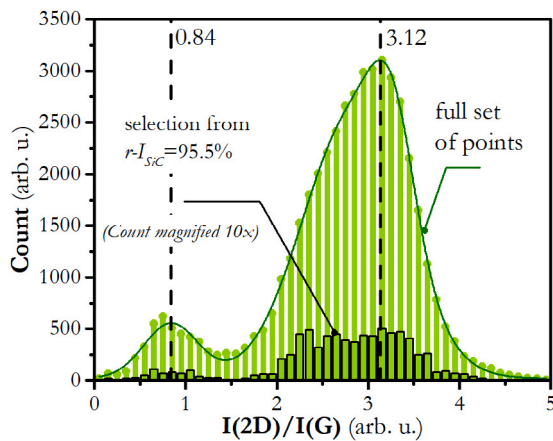


Fig. 7. Histogram of 2D-to-G band intensity ratio originating from the 20- μm \times 10- μm 5151-point Raman maps collected in ten evenly distributed test structures featuring a cross-shaped 100- μm \times 300- μm hydrogen-intercalated QFS epitaxial CVD graphene mesa on semi-insulating vanadium-compensated on-axis 6H-SiC(0001). Marked out with a black rim is data associated with $r - I_{SiC} = 95.5\%$ (1L*).

relative intensity $r - I_{SiC} = 95.5\%$ and thus denoted truly single-layer (1L*) span a narrower yet still relatively broad range between 47 cm⁻¹ and 60 cm⁻¹ (Fig. 6).

The distribution of the 2D-to-G band intensity ratio exposes two peaks, one at $I_{2D}/I_G = 0.84$ and the other at $I_{2D}/I_G = 3.12$. The three-fold ratio is consistent with the low value of N derived from the functional Raman analysis and the spectroscopic ellipsometry. The sub-unity ratio may likely be associated with the vestigial presence of SiC step edges (Fig. 7).

Plotted against Lee's graphical representation of (ω_G , ω_{2D}) in p-doped single-layer micromechanically exfoliated graphene transferred onto a SiO₂/Si substrate and characterized with a 532-nm laser line [45], the data points form an elongated cloud positioned outside of the original half-plane (gray area in Fig. 8). The cloud is located between $\omega_G = 1585$ cm⁻¹ and $\omega_G = 1605$ cm⁻¹, and $\omega_{2D} = 2690$ cm⁻¹ and $\omega_{2D} = 2730$ cm⁻¹. Individual points associated with $r - I_{SiC} = 95.5\%$ form a narrower set, limited to ω_G^{1L*} between 1586 cm⁻¹ and 1597 cm⁻¹, and ω_{2D}^{1L*} between 2695 cm⁻¹ and 2725 cm⁻¹. The narrower set is inclined at an angle of $\text{tg}(\alpha) = 2.1$, which is almost identical to the $\text{tg}(\alpha) = 2.2$ characterizing the lines of constant hole concentration in Lee's half-plane.

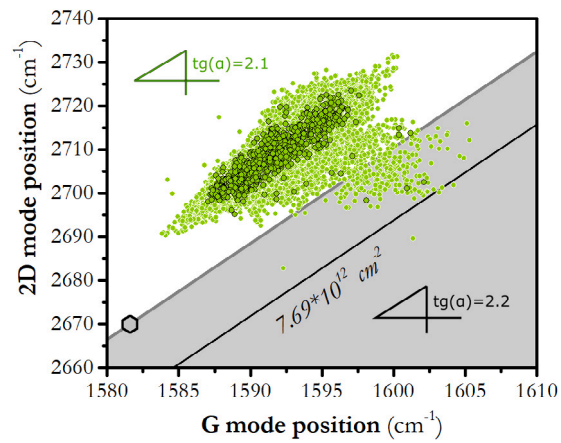


Fig. 8. Data cloud of the G and 2D band positions originating from the 20- μm \times 10- μm 5151-point Raman maps collected in ten evenly distributed test structures featuring a cross-shaped 100- μm \times 300- μm hydrogen-intercalated QFS epitaxial CVD graphene mesa on semi-insulating vanadium-compensated on-axis 6H-SiC(0001). Marked out with black circles is data associated with $r - I_{SiC} = 95.5\%$ (1L*). The points are plotted against Lee's half-plane (marked in gray), defining limits for p-doped single-layer micromechanically exfoliated graphene transferred onto a SiO₂/Si substrate. The gray hexagon represents undoped and unstrained graphene on SiO₂/Si. Drawn with black is the line of constant hole concentration $p_s = 7.69 \times 10^{12}$ cm⁻² for graphene on SiO₂/Si.

We believe the non-functional micro-Raman analysis based on A_{2D} , I_{2D}/I_G , and (ω_G, ω_{2D}) is not universal and unambiguous as it lacks the formalism applied in the analysis of $r - I_{SiC}$ and Ψ . For this reason, we disclose the data but refrain from interpreting them and concluding on the number of the graphene layers N .

Of no assistance is also the International Electrotechnical Commission Technical Standard No. 62607-6-6:2021. Although this document suggests that the A_{2D} should serve as a figure of merit to quantify graphene quality based on the experimental observation that the 2D peak width correlates with nanometer-scale strain variations - a scattering mechanism identified as dominant in the suppression of the charge carrier mobility [46], it does not provide formalism to calculate the N .

3.5. High-resolution transmission electron microscopy

The 10-nm-long HR-TEM image appears to confirm the above-evoked discussion on the presence of one QFS layer of graphene against hydrogen-saturated semi-insulating vanadium-compensated 6H-SiC (0001). For visual clarity, the cross-sectional figure is supported with a simulation of the expected TEM image (Fig. 9).

4. Conclusions

In this report, we grew transfer-free p-type hydrogen-intercalated quasi-free-standing epitaxial Chemical Vapor Deposition graphene on 15-mm \times 15-mm semi-insulating vanadium-compensated on-axis 6H-SiC(0001). The graphene is characterized in that its room-temperature direct-current Hall-effect-derived hole mobility $\mu_p = 5019$ cm²/Vs, which falls within the 90th percentile of our historical production stock.

The statistical number of the graphene layers, as derived from the distribution of the relative intensity of the SiC-related Raman-active longitudinal optical A_1 mode at 964 cm⁻¹ $r - I_{SiC}$, is $N = 1.05$. In the domain of the spectroscopic angle Ψ measured at AOI = 50° and $\lambda = 490$ nm, the QFS graphene spans the range between $\Psi = 25.9^\circ$ and $\Psi = 26.9^\circ$, with the distribution peak at $\Psi = 26.35^\circ$. Its presence up-shifts Ψ by 0.33° versus exposed 6H-SiC(0001), which was associated with statistically $N = 0.97$ layers. The close-to-unity value of N made us conclude that the graphene is a close-to-perfect QFS monolayer.

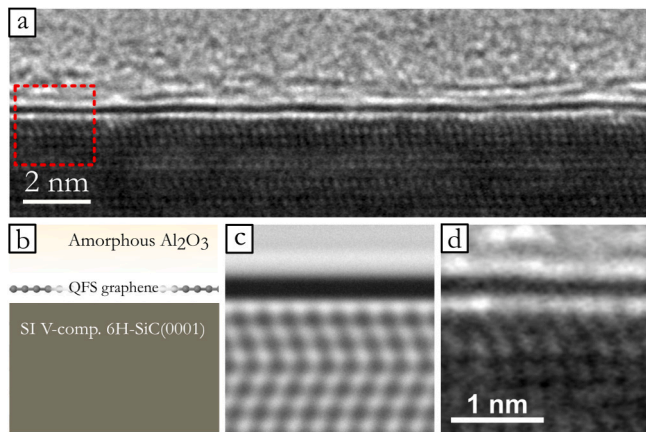


Fig. 9. (a) High-Resolution Transmission Electron Microscope cross-sectional image of the aluminum-oxide-passivated hydrogen-intercalated QFS epitaxial CVD graphene on semi-insulating vanadium-compensated on-axis 6H-SiC(0001). The amorphous Al_2O_3 passivation played no role but to secure the structural composition of graphene throughout the process of the thin Pt layer deposition. (b) Schematic of the material structure. (c) Simulation of the TEM image. (d) Actual close-up of the $2\text{ nm} \times 2\text{ nm}$ area marked with a red dashed line in sub-figure (a).

In the domain of the spectroscopic angle Δ measured at $\text{AOI} = 50^\circ$ and $\lambda = 490 \text{ nm}$, the QFS graphene spans the range between $\Delta = 172.2^\circ$ and $\Delta = 173.1^\circ$, with the histogram peak at $\Delta = 172.63^\circ$. Its presence up-shifts Δ by 1.60° versus exposed 6H-SiC(0001).

Non-functional Raman analysis revealed that the average 2D peak width $\Delta_{2D} = 53.6 \text{ cm}^{-1}$, and the dominant 2D-to-G band intensity ratio $I_{2D}/I_G = 3.12$. In the domain of the band positions, the material stretches from $\omega_G = 1585 \text{ cm}^{-1}$ to $\omega_G = 1605 \text{ cm}^{-1}$ and from $\omega_{2D} = 2690 \text{ cm}^{-1}$ to $\omega_{2D} = 2730 \text{ cm}^{-1}$.

A high-resolution Transmission Electron Microscope image exposed a single QFS layer of graphene against hydrogen-saturated semi-insulating vanadium-compensated on-axis 6H-SiC(0001). The authors conclude that the close-to-unity value of N , supported by the high value of hole mobility and the HR-TEM image, prove that the material under study is a close-to-perfect QFS monolayer and, therefore, its spectroscopic properties $r - I_{\text{SiC}}$, Ψ , Δ , Δ_{2D} , I_{2D}/I_G , and (ω_G, ω_{2D}) constitute a valuable reference for this class of materials.

CRediT authorship contribution statement

Artur Dobrowolski: Conceptualization, Investigation, Data curation, Writing – original draft, Visualization. **Jakub Jagiełło:** Conceptualization, Investigation, Writing – original draft. **Karolina Piętak-Jureczak:** Conceptualization, Investigation, Writing – original draft. **Marek Wzorek:** Investigation. **Dariusz Czołak:** Resources. **Tymoteusz Ciuk:** Conceptualization, Writing – original draft, Writing – review & editing, Supervision.

Declaration of competing interest

The authors declare that they have no known competing financial interests or personal relationships that could have appeared to influence the work reported in this paper.

Data availability

Data will be made available on request.

Acknowledgments

The research leading to these results has received funding from the National Science Centre, Poland, under Grant Agreement No. OPUS 2019/33/B/ST3/02677 for the project “Influence of the silicon carbide and the dielectric passivation defect structure on high-temperature electrical properties of epitaxial graphene” and under Grant Agreement No. PRELUDIUM 2022/45/N/ST5/02273 for the project “The synthesis of aluminium oxide passivation for the precise modification of the physico-chemical properties of graphene”. The research has also been supported by the National Centre for Research and Development, Poland, under Grant Agreement No. M-ERA.NET3/2021/83/I4BAGS/2022 for the project “Ion Implantation for Innovative Interface modifications in BAttery and Graphene-enabled Systems”. The M-ERA.NET3 has received funding from the European Union’s Horizon 2020 research and innovation programme under Grant Agreement No. 958174.

References

- [1] C. Riedl, C. Coletti, T. Iwasaki, A.A. Zakharov, U. Starke, Quasi-free-standing epitaxial graphene on SiC obtained by hydrogen intercalation, *Phys. Rev. Lett.* 103 (24) (2009).
- [2] S. Watcharinayon, C. Virojanadara, J. Osiecki, A. Zakharov, R. Yakimova, R. Uhrberg, L. Johansson, Hydrogen intercalation of graphene grown on 6H-SiC(0001), *Surf. Sci.* 605 (17–18) (2011) 1662–1668.
- [3] J.D. Emery, V.D. Wheeler, J.E. Johns, M.E. McBriarty, B. Detlefs, M.C. Hersam, D.K. Gaskill, M.J. Bedzyk, Structural consequences of hydrogen intercalation of epitaxial graphene on SiC(0001), *Appl. Phys. Lett.* 105 (16) (2014) 161602.
- [4] J. Sołtyś, J. Piechota, M. Ptasińska, S. Kruckowski, Hydrogen intercalation of single and multiple layer graphene synthesized on si-terminated SiC(0001) surface, *J. Appl. Phys.* 116 (8) (2014) 083502.
- [5] M.J. Szary, S. El-Ahmar, T. Ciuk, The impact of partial h intercalation on the quasi-free-standing properties of graphene on SiC(0001), *Appl. Surf. Sci.* 541 (2021) 148668.
- [6] W. Strupiński, K. Grodecki, A. Wysmolek, R. Stepniewski, T. Szkopek, P.E. Gaskill, A. Grüneis, D. Haberer, R. Bozek, J. Krupka, J.M. Baranowski, Graphene epitaxy by chemical vapor deposition on SiC, *Nano Lett.* 11 (4) (2011) 1786–1791.
- [7] T. Ciuk, W. Strupiński, Statistics of epitaxial graphene for Hall effect sensors, *Carbon* 93 (2015) 1042–1049.
- [8] T. Ciuk, P. Caban, W. Strupiński, Charge carrier concentration and offset voltage in quasi-free-standing monolayer chemical vapor deposition graphene on SiC, *Carbon* 101 (2016) 431–438.
- [9] T. Ciuk, A. Kozłowski, P.P. Michałowski, W. Kaszub, M. Kozubal, Z. Rekuc, J. Podgorski, B. Stanczyk, K. Przyborowska, I. Jozwik, A. Kowalik, P. Kamiński, Thermally activated double-carrier transport in epitaxial graphene on vanadium-compensated 6H-SiC as revealed by Hall effect measurements, *Carbon* 139 (2018) 776–781.
- [10] T. Ciuk, B. Stanczyk, K. Przyborowska, D. Czołak, A. Dobrowolski, J. Jagiełło, W. Kaszub, M. Kozubal, R. Kozłowski, P. Kamiński, High-temperature Hall effect sensor based on epitaxial graphene on high-purity semiinsulating 4H-SiC, *IEEE Trans. Electron Devices* 66 (7) (2019) 3134–3138.
- [11] A. Dobrowolski, J. Jagiełło, D. Czołak, T. Ciuk, Determining the number of graphene layers based on Raman response of the SiC substrate, *Physica E* 134 (May) (2021) 114853.
- [12] O. Habibpour, Z.S. He, W. Strupiński, N. Rorsman, T. Ciuk, P. Ciepielewski, H. Zirath, Graphene FET gigabit ON-OFF keying demodulator at 96 GHz, *IEEE Electron Device Lett.* 37 (3) (2016) 333–336.
- [13] O. Habibpour, Z.S. He, W. Strupiński, N. Rorsman, H. Zirath, Wafer scale millimeter-wave integrated circuits based on epitaxial graphene in high data rate communication, *Sci. Rep.* 7 (1) (2017).
- [14] O. Habibpour, Z.S. He, W. Strupiński, N. Rorsman, T. Ciuk, P. Ciepielewski, H. Zirath, A W-band MMIC resistive mixer based on epitaxial graphene FET, *IEEE Microw. Wirel. Compon. Lett.* 27 (2) (2017) 168–170.
- [15] S. El-Ahmar, M.J. Szary, T. Ciuk, R. Prokopowicz, A. Dobrowolski, J. Jagiełło, M. Ziembia, Graphene on SiC as a promising platform for magnetic field detection under neutron irradiation, *Appl. Surf. Sci.* 590 (2022) 152992.
- [16] T. Ciuk, S. Cakmakyan, E. Ozbay, P. Caban, K. Grodecki, A. Krajewska, I. Pasternak, J. Szmidt, W. Strupiński, Step-edge-induced resistance anisotropy in quasi-free-standing bilayer chemical vapor deposition graphene on SiC, *J. Appl. Phys.* 116 (12) (2014) 123708.
- [17] T. Ciuk, W. Kaszub, K. Kosciewicz, A. Dobrowolski, J. Jagiełło, A. Chamryga, J. Gaca, M. Wojcik, D. Czołak, B. Stanczyk, K. Przyborowska, R. Kozłowski, M. Kozubal, P.P. Michałowski, M.J. Szary, P. Kamiński, Highly-doped p-type few-layer graphene on UID off-axis homoepitaxial 4H-SiC, *Curr. Appl. Phys.* 27 (2021) 17–24.

- [18] K. Piętak, J. Jagiełło, A. Dobrowolski, R. Budzich, A. Wysmolek, T. Ciuk, Enhancement of graphene-related and substrate-related Raman modes through dielectric layer deposition, *Appl. Phys. Lett.* 120 (6) (2022) 063105.
- [19] A. Dobrowolski, J. Jagiełło, T. Ciuk, K. Piętak, E.B. Mozdzyńska, Layer-resolved Raman imaging and analysis of parasitic ad-layers in transferred graphene, *Appl. Surf. Sci.* 608 (2023) 155054.
- [20] R.R. Nair, P. Blake, A.N. Grigorenko, K.S. Novoselov, T.J. Booth, T. Stauber, N.M.R. Peres, A.K. Geim, Fine structure constant defines visual transparency of graphene, *Science* 320 (5881) (2008) 1308.
- [21] C. Berger, Z. Song, T. Li, X. Li, A.Y. Ogbazghi, R. Feng, Z. Dai, A.N. Marchenkov, E.H. Conrad, P.N. First, W.A. de Heer, Ultrathin epitaxial graphite: 2D electron gas properties and a route toward graphene-based nanoelectronics, *J. Phys. Chem. B* 108 (52) (2004) 19912–19916.
- [22] J. Hass, W.A. de Heer, E.H. Conrad, The growth and morphology of epitaxial multilayer graphene, *J. Phys.: Condens. Matter* 20 (32) (2008) 323202.
- [23] K.V. Emtsev, A. Bostwick, K. Horn, J. Jobst, G.L. Kellogg, L. Ley, J.L. McChesney, T. Ohta, S.A. Reshanov, J. Röhrl, E. Rotenberg, A.K. Schmid, D. Waldmann, H.B. Weber, T. Seyller, Towards wafer-size graphene layers by atmospheric pressure graphitization of silicon carbide, *Nature Mater.* 8 (3) (2009) 203–207.
- [24] S. Chen, M.H. von Hoegen, P.A. Thiel, M.C. Tringides, Diffraction paradox: An unusually broad diffraction background marks high quality graphene, *Phys. Rev. B* 100 (15) (2019).
- [25] T. Ciuk, O. Petruk, A. Kowalik, I. Jozwik, A. Rychter, J. Szmidt, W. Strupinski, Low-noise epitaxial graphene on SiC Hall effect element for commercial applications, *Appl. Phys. Lett.* 108 (22) (2016) 223504.
- [26] A. Krajewska, I. Pasternak, G. Sobon, J. Sotor, A. Przewloka, T. Ciuk, J. Sobieski, J. Grzonka, K. Abramski, W. Strupinski, Fabrication and applications of multi-layer graphene stack on transparent polymer, *Appl. Phys. Lett.* 110 (2017) 041901.
- [27] S. Nakashima, H. Harima, Raman investigation of SiC polytypes, *Phys. Status Solidi (A) Appl. Mater. Sci.* 162 (39) (1997) 39–64.
- [28] C. Bouhafs, V. Darakchieva, I.L. Persson, A. Tiberj, P.O.Å. Persson, M. Paillet, A.-A. Zahab, P. Landois, S. Juillaguet, S. Schöche, M. Schubert, R. Yakimova, Structural properties and dielectric function of graphene grown by high-temperature sublimation on 4H-SiC(0001), *J. Appl. Phys.* 117 (8) (2015) 085701.
- [29] A. Boosalis, T. Hofmann, V. Darakchieva, R. Yakimova, M. Schubert, Visible to vacuum ultraviolet dielectric functions of epitaxial graphene on 3C and 4H SiC polytypes determined by spectroscopic ellipsometry, *Appl. Phys. Lett.* 101 (1) (2012) 011912.
- [30] E. Widianto, V. Efelia, K. Megasari, A. Kusumaatmaja, K. Triyana, A. Rusydi, I. Santoso, Calculation of refractive index of multilayer epitaxial graphene on C-face SiC measured by synchrotron using kramers-kronig and Newton-raphson method, in: AIP Conference Proceedings, Author(s), 2016.
- [31] I. Santoso, S.L. Wong, X. Yin, P.K. Gogoi, T.C. Asmara, H. Huang, W. Chen, A.T.S. Wee, A. Rusydi, Optical and electronic structure of quasi-freestanding multilayer graphene on the carbon face of SiC, *EPL (Europhys. Lett.)* 108 (3) (2014) 37009.
- [32] R. Yakimova, T. Iakimov, G. Yazdi, C. Bouhafs, J. Eriksson, A. Zakharov, A. Boosalis, M. Schubert, V. Darakchieva, Morphological and electronic properties of epitaxial graphene on SiC, *Physica B* 439 (2014) 54–59.
- [33] V. Darakchieva, A. Boosalis, A.A. Zakharov, T. Hofmann, M. Schubert, T.E. Tiwald, T. Iakimov, R. Vasiliauskas, R. Yakimova, Large-area microfocal spectroscopic ellipsometry mapping of thickness and electronic properties of epitaxial graphene on Si- and C-face of 3C-SiC(111), *Appl. Phys. Lett.* 102 (21) (2013) 213116.
- [34] R. Yakimova, G.R. Yazdi, T. Iakimov, J. Eriksson, V. Darakchieva, Challenges of graphene growth on silicon carbide, *ECS Trans.* 53 (1) (2013) 9–16.
- [35] F. Nelson, D.P. Sinha, E. Comfort, J.U. Lee, A.C. Diebold, A. Sandin, D.B. Dougherty, J.E. Rowe, Aberration corrected microscopy of CVD graphene and spectroscopic ellipsometry of epitaxial graphene and CVD graphene for comparison of the dielectric function, *ECS Trans.* 45 (4) (2012) 63–71.
- [36] K. Megasari, E. Widianto, V. Efelia, K. Abraha, A.T.S. Wee, A. Rusydi, I. Santoso, Calculation of dielectric constant of buffer layer graphene on SiC measured by spectroscopy ellipsometry using Gauss-Newton numerical inversion method, in: AIP Conference Proceedings, Author(s), 2016.
- [37] F. Nelson, A. Sandin, D.B. Dougherty, D.E. Aspnes, J.E. Rowe, A.C. Diebold, Optical and structural characterization of epitaxial graphene on vicinal 6H-SiC(0001)-si by spectroscopic ellipsometry, auger spectroscopy, and STM, *J. Vac. Sci. Technol. B, Nanotechnol. Microelectron.: Mater., Process., Meas., Phenom.* 30 (4) (2012) 04E106.
- [38] P.E. Gaskell, H.S. Skulason, W. Strupinski, T. Szkopek, High spatial resolution ellipsometer for characterization of epitaxial graphene, *Opt. Lett.* 35 (20) (2010) 3336.
- [39] T. Ciuk, Ł. Ciura, P. Michałowski, J. Jagiełło, A. Dobrowolski, K. Piętak, D. Kalita, M. Wzorek, R. Budzich, D. Czołak, A. Kolek, Contamination-induced inhomogeneity of noise sources distribution in Al_2O_3 -passivated quasi-free-standing graphene on 4H-SiC(0001), *Physica E: Low-Dimens. Syst. Nanostruct.* 142 (2022) 115264.
- [40] J. Ristein, S. Mammadov, T. Seyller, Origin of doping in quasi-free-standing graphene on silicon carbide, *Phys. Rev. Lett.* 108 (24) (2012).
- [41] S. Mammadov, J. Ristein, R.J. Koch, M. Ostler, C. Raidel, M. Wanke, R. Vasiliauskas, R. Yakimova, T. Seyller, Polarization doping of graphene on silicon carbide, *2D Mater.* 1 (3) (2014) 035003.
- [42] J. Śląwińska, H. Aramberri, M. Muñoz, J. Cerdá, Ab initio study of the relationship between spontaneous polarization and p-type doping in quasi-freestanding graphene on H-passivated SiC surfaces, *Carbon* 93 (2015) 88–104.
- [43] C. Thomsen, S. Reich, Double resonant Raman scattering in graphite, *Phys. Rev. Lett.* 85 (24) (2000) 5214–5217.
- [44] A.C. Ferrari, J.C. Meyer, V. Scardaci, C. Casiraghi, M. Lazzeri, F. Mauri, S. Pisacane, D. Jiang, K.S. Novoselov, S. Roth, A.K. Geim, Raman spectrum of graphene and graphene layers, *Phys. Rev. Lett.* 97 (2006) 187401.
- [45] J.E. Lee, G. Ahn, J. Shim, Y.S. Lee, S. Ryu, Optical separation of mechanical strain from charge doping in graphene, *Nature Commun.* 3 (1) (2012).
- [46] N.J. Couto, D. Costanzo, S. Engels, D.-K. Ki, K. Watanabe, T. Taniguchi, C. Stampfer, F. Guinea, A.F. Morpurgo, Random strain fluctuations as dominant disorder source for high-quality on-substrate graphene devices, *Phys. Rev. X* 4 (4) (2014).